

Nanoscale, Electrified Liquid Jets for High-Resolution Printing of Charge

Jang-Ung Park,^{†,‡,||} Sangkyu Lee,^{†,‡,§} Sakulsuk Unarunotai,[†] Yugang Sun,[§] Simon Dunham,[†] Taeseup Song,[†] Placid M. Ferreira,[†] Andrew G. Alleyene,[†] Ungyu Paik,^{*,‡} and John A. Rogers^{*,†}

[†]Department of Materials Science & Engineering, Department of Chemistry, Department of Mechanical Science and Engineering, Beckman Institute, and Frederick Seitz Materials Research Laboratory, University of Illinois at Urbana–Champaign, Urbana, Illinois 61801, [‡]Division of Materials Science Engineering, Department of Energy Engineering, Hanyang University, Seoul 133-791, Republic of Korea, and [§]Center for Nanoscale Materials, Argonne National Laboratory, Argonne, Illinois 60439

ABSTRACT Nearly all research in micro- and nanofabrication focuses on the formation of solid structures of materials that perform some mechanical, electrical, optical, or related function. Fabricating patterns of charges, by contrast, is a much less well explored area that is of separate and growing interest because the associated electric fields can be exploited to control the behavior of nanoscale electronic and mechanical devices, guide the assembly of nanomaterials, or modulate the properties of biological systems. This paper describes a versatile technique that uses fine, electrified liquid jets formed by electrohydrodynamics at micro- and nanoscale nozzles to print complex patterns of both positive and negative charges, with resolution that can extend into the submicrometer and nanometer regime. The reported results establish the basic aspects of this process and demonstrate the capabilities through printed patterns with diverse geometries and charge configurations in a variety of liquid inks, including suspensions of nanoparticles and nanowires. The use of printed charge to control the properties of silicon nanomembrane transistors provides an application example.

KEYWORDS Electrohydrodynamics, jet printing, charge printing, electrostatic doping, semiconductor nanomaterials

The most widespread use of charge patterning is in xerography,^{1,2} where a corona creates uniform electrostatic charge on the surface of a photoconductor; patterned exposure of light then leads to local charge dissipation in desired geometries. The resulting pattern of charge guides the assembly of toner particles (with opposite charge) that are subsequently sintered to form a permanent image. Recently, more research-oriented techniques have been developed to allow considerably higher resolution and finer control over charge, by use of conducting tips in the form of either atomic force microscope (AFM) probes,^{3–8} or metal-coated elastomeric stamps,^{9–11} both in contact printing schemes. The process involves injection of electrons into materials such as poly(methyl methacrylate) and SiO₂ that can store this charge for extended periods (i.e., via formation of electrets). In these existing techniques, specialized materials for the photoconductors and electrets^{9,12,13} are required, thereby limiting their broader utility. Here we report a much different approach that involves the direct printing of ions from fine nozzle tips in the form of electrified liquid jets with nanoscale dimensions. Positive and negative pat-

terns of ionic charge, with nanoscale resolution and in nearly arbitrary configurations, can be formed in this manner.

The experimental setups rely on adapted versions of electrohydrodynamic jet (e-jet) printers^{14–16} that were recently reported as high-resolution alternatives to conventional thermal and piezoelectric inkjet systems. Such technology enables printing of liquid inks with resolution approaching ~100 nm for applications in DNA microarrays, printed transistors, biosensors, and fine electrode structures.^{14–17} In these systems, ink delivered from a reservoir to the tip of a fine, metal-coated nozzle forms a pendent hemispherical meniscus. A dc voltage bias applied between the nozzle and the substrate leads to the accumulation of mobile charges in the ink near the surface of the meniscus, as illustrated in Figure 1a. Positive (negative) charges predominate with positive (negative) voltages at the nozzle relative to those at the substrate. Coulombic repulsion between these charges induces electrostatic stresses that deform the meniscus into a conical shape (Taylor cone).¹⁸ With increasing applied voltage, the sum of this electrostatic force and the externally applied pressure eventually exceeds the force associated with the capillary pressure at the apex of the cone, leading to the formation of a thin liquid jet that emerges from the tip of the Taylor cone and ejects toward the substrate.^{19–22} (A constant, externally applied pressure (e.g., pneumatic) can assist the electric-field-induced liquid flow.¹⁶) Figure 1b shows an image of a representative conical meniscus, a liquid jet, and printed droplet, captured using a

* To whom correspondence should be addressed: (J.A.R.) jrogers@illinois.edu; (U.P.) upaik@hanyang.ac.kr.

† These authors are contributed equally to this work.

|| Current address: Department of Chemistry and Chemical Biology, Harvard University, Cambridge, MA 02138.

Received for review: 10/20/2009

Published on Web: 01/12/2010

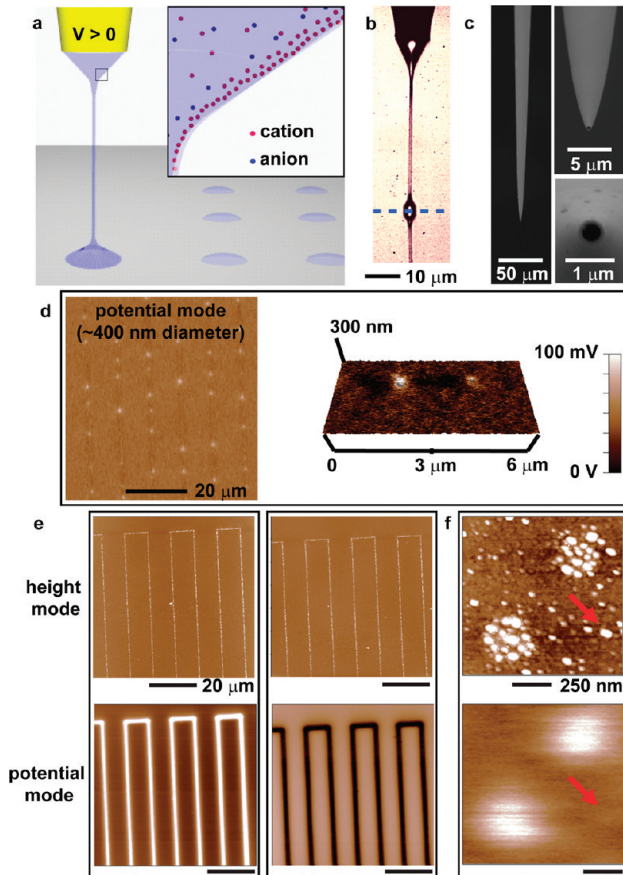


FIGURE 1. High-resolution printing of charge by controlled use of electrohydrodynamic jets (e-jets). (a) Schematic illustration of field-induced charge accumulation near the meniscus at the tip of a fine nozzle. (b) Cone-jet transition captured using a high-speed camera. The image reflected from a substrate (blue dashed line) is also shown. (c) SEM images (side and tip view) of a nozzle with 300 nm internal diameter (i.d.). (d) KFM potential image (left) and the 3D image (right) that includes height information. (e) KFM height (top) and potential (bottom) mode images of the patterns printed using the 300 nm i.d. nozzle at PPM (left) and NPM (right). Here, the dot diameters are $\sim 300\text{--}400\text{ nm}$ in the height mode. (f) KFM images of the charged dots printed using a spray mode. A printed dot was indicated with a red arrow to show the limit of our KFM potential measurement, as an example.

high-speed camera (Phantom v7.0, Vision Research). After ejection, the jet retracts back to the nozzle, to recover the original meniscus shape.^{14,23} A key, previously unexploited feature of this process is that the printed droplets contain overall net charge. Here we demonstrate that this physics can be exploited to yield a “charge printer” capable of forming complex patterns of positive or negative (or both) ionic charge with resolution extending into the nanoscale regime, with very little or controlled amounts of material transfer, on nearly any surface. Application possibilities range from invisible, printed security codes to means for electrostatic control of nanoelectronic/mechanical devices to guided assembly of charged particles or micro/nanostructures to modulation of activity in biological systems. In the following, we describe the fundamental aspects and the technical capabilities, with an application example in the

controlled, patterned electrostatic doping of silicon nanomembrane transistors.

As an example, panels c and d of Figure 1 show a scanning electron microscope (SEM) image of a nozzle tip with a 300 nm i.d. and dots of charge ($\sim 400\text{ nm}$ diameters) printed with such a nozzle, respectively. Here, the ink consisted of a photocurable polyurethane (NOA 74, Norland) and the substrate was SiO_2 (100 nm)/Si treated with hexamethyldisilazane (HMDS). The left frames of Figure 1e correspond to jetting with a positive voltage at the nozzle and a grounded substrate, which we will refer to in the following as the positive printing mode (PPM). Kelvin force microscopy (KFM; height and potential modes, Asylum research MFP-3D AFM) revealed that the printed dots have positive potentials (dot diameter, $\sim 300\text{ nm}$ in height modes; charge width, $\sim 2.5\text{ }\mu\text{m}$ in potential mode) as expected from the physics of the process outlined in the previous paragraph. Here, the peak potentials are ca. +1 V, at the position of the thickest regions ($\sim 15\text{ nm}$) of the printed dots. Reversing the bias yields nearly identical printing resolution, but with opposite charge (right of Figure 1e). We refer to this operation as negative printing mode (NPM). Although the ultimate limits in resolution are difficult to define, we suspect that they extend to the range of tens of nanometers and below. As evidence, Figure 1f shows printed droplets and charge formed at the periphery of an area patterned in a high-voltage operating mode designed to produce some spray. Here, the feature sizes (i.e., 40–80 nm of dot diameters in the height mode) approach the limits associated with our KFM measurement.

In addition to nanoscale features, these methods are well suited to the patterned deposition of nanomaterials with controlled charge. Figure 2a shows examples of the silver nanoparticles (2–5 nm diameter) with a proprietary organic functional group for dispersion in tetradecane (Harima Chemicals, NPS-J-HP). Lines were printed using the ink with PPM (top) and NPM (bottom); the peak potentials were ca. $\pm 0.5\text{ V}$ with $\sim 10\text{ nm}$ heights (nozzle, 1 μm i.d.). Panels b and c of Figure 2 represent the potential images of patterns printed using suspensions of silver nanowires²⁴ and nanocubes³⁵ (50 wt % of dimethylformamide added for nanowires and nanocubes) with 5 μm i.d. nozzles. Here, the nanowires (diameter, $\sim 60\text{ nm}$; length, $\sim 10\text{ }\mu\text{m}$) and nanocubes (edge length, $\sim 120\text{ nm}$) were printed with organic residues; the peak potentials of the dots are ca. ± 0.3 and $\pm 0.7\text{ V}$, respectively. Use of these or other inks with automated e-jet printer systems allows formation of user-definable charge patterns. Figure 2d provides KFM analysis of an image of Michelangelo’s piéta statue formed in PPM with a 500 nm i.d. nozzle and polyurethane ink. The total size of the image is $\sim 800 \times 820\text{ }\mu\text{m}$, as shown in the left side of Figure 2d. The physical heights (peak values $\sim 150\text{ nm}$) of the dots in the red-dashed area and their electrical potentials (peak values $\sim 0.25\text{ V}$) appear in the right side of Figure 2d. We note that for these inks, and in certain other cases that

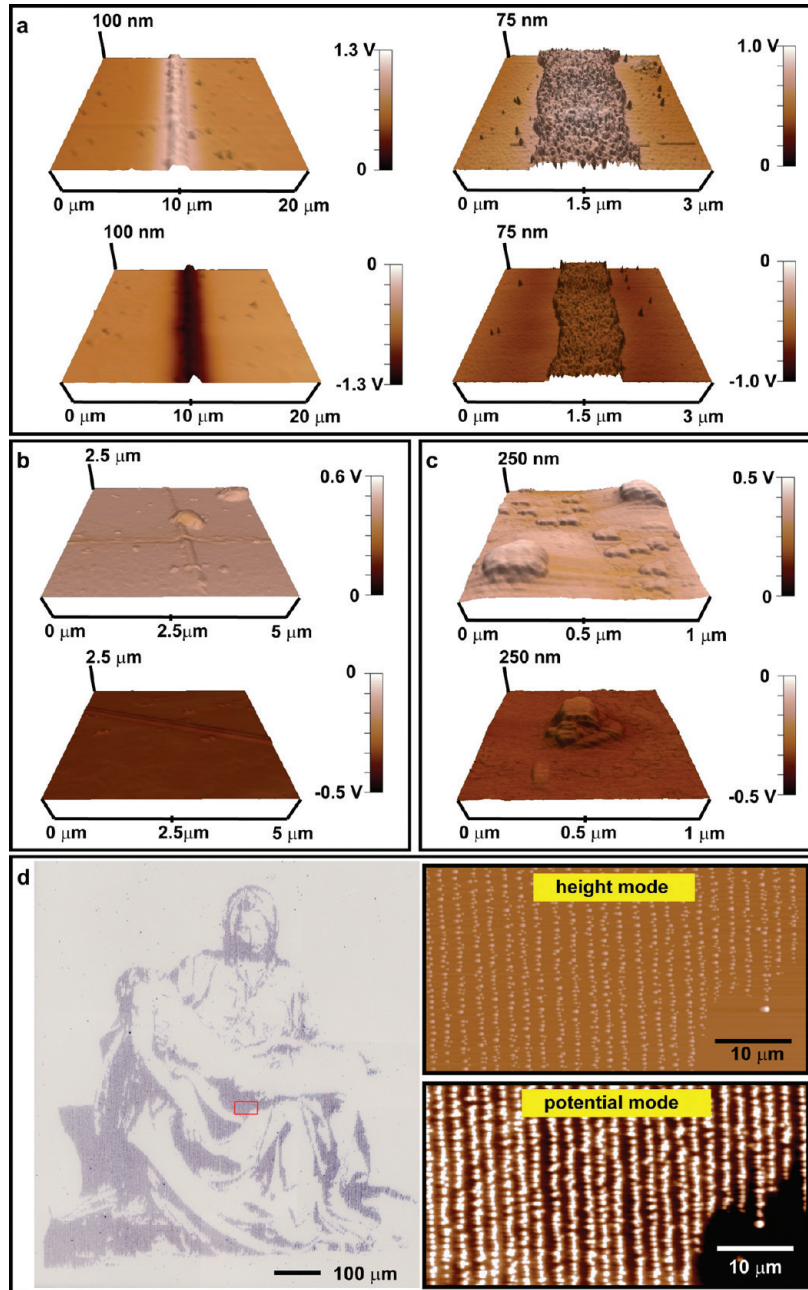


FIGURE 2. Charge printing using various inks, including nanomaterials, in simple and complex geometries. 3D KFM images of the samples printed using suspensions of (a) Ag nanoparticles, (b) Ag nanowires, and (c) Ag nanocubes at PPM (top) and NPM (bottom). Right images in (a) show magnified areas. (d) Optical micrograph of a complex pattern (Michelangelo's pieta) of charge printed by e-jet using a polyurethane ink (left), with high-resolution images of height (AFM; top) and potential (KFM; bottom) corresponding to the red box on the left. The peak thicknesses and potentials associated with the dots in these images are ~ 150 nm and ~ 0.25 V, respectively.

follow, we did not add ionic components. Residual concentrations of ions are apparently sufficient. The breakup of a droplet occurs when the electrostatic repulsion exceeds the surface tension.²⁵ The maximum amount of charge per droplet is therefore limited, and dependent on the droplet size as well as surface tension of the liquid–air interface (Rayleigh limit).^{25–27} In e-jet, the characteristic droplet size can be changed by changing the nozzle diameter or the applied air pressure,^{16,23} thereby providing also a means to

control the charge printed in each drop. To demonstrate this effect, we printed dots with different diameters and then determined their potentials with KFM. As shown in Figure S1 in Supporting Information, bigger droplets printed with higher air pressures lead to larger potentials.

As illustrated in Figure 1, switching the direction of the electric field used to initiate jetting reverses the charge of the printed droplets. Controlling the bias during printing allows formation of patterns with both charge polarities.

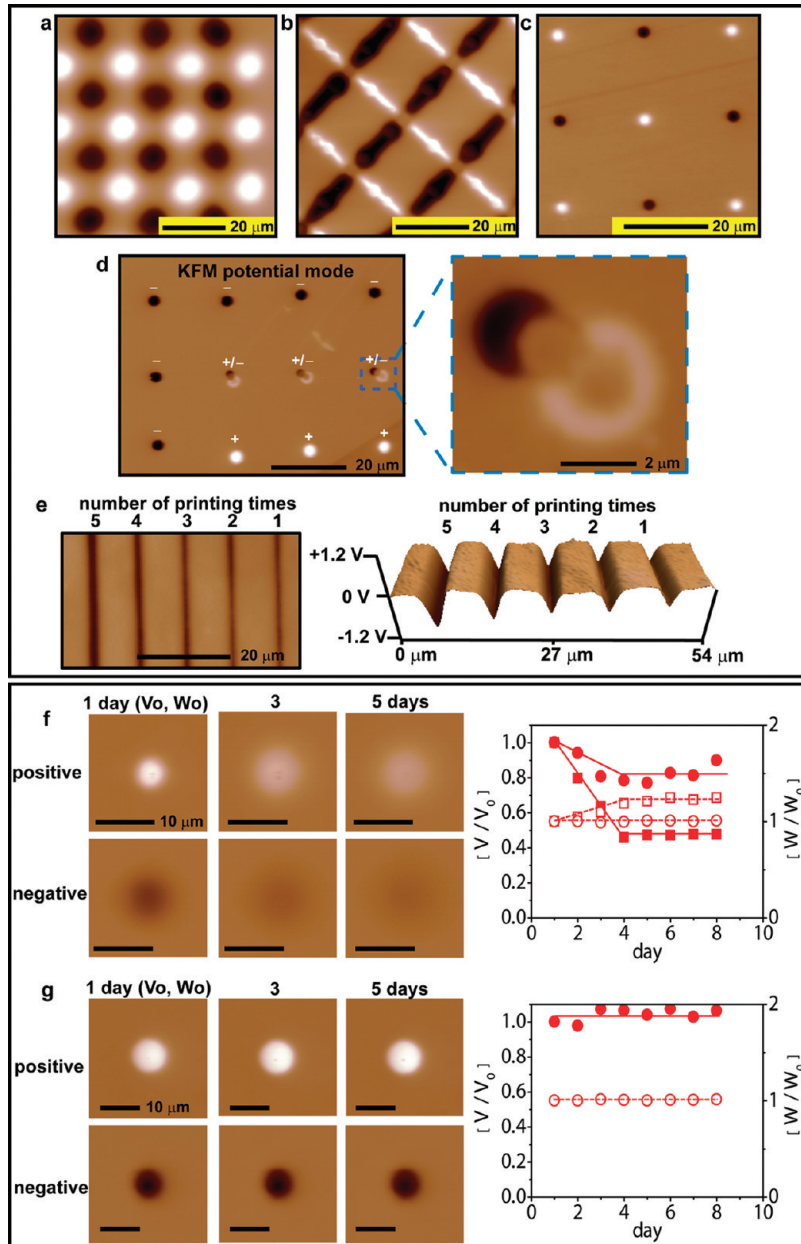


FIGURE 3. Printing and dissipation of positive and negative charges controlled by electric field direction. (a) Potential mode KFM images of aqueous sodium phosphate solution (10 mM, pH \sim 7). (b) Polyurethane (pH \sim 5). (c) Quinoline (pH $>$ 8). (d) Aqueous DNA suspension. (e) Potential control by printing multiple times with an ink of (poly(ethylene glycol) diacrylate). (f) KFM potential images of an ink of NaCl in water (30% glycerin added), printed on a 100 nm thick SiO₂ surface (on a Si wafer) in ambient air with a 2 μ m i.d. nozzle, at various times after printing. The graph on the right shows the change in characteristic widths (W) and peak potentials (V), normalized to the values immediately after printing (W_0 , V_0), for the positive case. The negative case shows similar behavior. The filled and vacant squares (or circles) in the graphs indicate the normalized potential (V/V_0) and fwhm (W/W_0) for the hydrophilic (or hydrophobic) surfaces, respectively. (g) KFM potential images of the NaCl ink printed stored in low humidity ($H_2O \sim 0.3$ ppm). The graph on the right provides information similar to that of the graph in the frame above.

Experiments show that in most practical cases of interest, the pre-existing patterns of charge have little effect on the printing process. As a result, various functional inks with a wide range of physical properties and pH values can be successfully printed in both PPM and NPM on a single substrate. Figure 3a shows patterns of dots with potentials of about +5.5 and -5.5 V (peak values), using an aqueous sodium phosphate solution (10 mM, pH \sim 7) as the ink.

Diameters and peak heights of dots with both polarities are \sim 10 μ m and \sim 90 nm, respectively. Figure 3b shows an array of lines patterned using the polyurethane ink (pH \sim 5). In this case, NPM yielded an array of charged lines at -1.3 V and then PPM yielded another set of lines +1.3 V oriented at right angles to the negative lines. In both cases, the line widths are \sim 3 μ m and thicknesses are less than 100 nm. At the crossing points, the negative and positive charges bal-

ance one another, thereby reducing the potentials in these regions to values close to 0 V. The material volumes add to yield heights of \sim 500 nm. Figure 3c shows a pattern of dots (\sim 3 μ m diameters; 7 nm heights) at ca. \pm 2.4 V (peak values) using an organic base, quinoline (pH >8) as the ink. An aqueous suspension of DNA (5 μ M) can be also printed in PPM and NPM, as shown in Figure 3d (left side); the negative and positive dots (\sim 3 μ m diameters and \pm 3.5 V peak values) are labeled (−) and (+), respectively. We used the single-stranded oligonucleotide (5'-Alexa546-ACT CAC TAT TTC GAC CGG CTC GGA GAA GAG ATG TCT C-3' (HPLC), Integrated DNA Technologies Inc.) suspended in H₂O without buffer but with 10 vol % of triethylene glycol to prevent nozzle clogging. The dots marked with “+/-” correspond to cases where droplets formed in PPM partially overlap (offset by \sim 2 μ m) with droplets from NPM. Here, the NPM operation occurred before complete drying of the PPM droplets, to facilitate some mixing. The potentials at and near the areas of overlap are significantly reduced, due to charge balance.

Printing in multiple passes with a common printing mode (i.e., NPM or PPM) increases the potential. As an example, charged lines printed using a 500 nm i.d. nozzle and an ink of poly(ethylene glycol) diacrylate (Sigma-Aldrich) (Figure 3e) exhibited potentials that scale with multiple printing cycles in the expected way, from ca. −0.2 V for a single pass to ca. −1 V for five cycles. Additional cycles can increase further the potentials, although sufficiently high values can affect jetting direction, stability,²⁸ and threshold voltages for printing.

Both positive and negative patterns of charge persist for times that depend on environmental factors including humidity and substrate properties such as hydrophobicity.^{9,12} We studied the dissipation of charges patterned by e-jet with an aqueous sodium chloride ink (1 mM, 30 wt % glycerin added to avoid nozzle clogging) on substrates of SiO₂/Si untreated and treated with HMDS. Panels f and g of Figure 3 present some results. In ambient conditions, the peak potentials decreased rapidly during the first few days due to lateral spreading of charge and then continued to decrease very slowly without significant additional spreading (curves of Figure 3f and Figure S2a in Supporting information). A sodium phosphate ink (1 mM, glycerin 30 wt %) also showed similar behaviors, as shown in Figure S3 in Supporting information. The temporal decay in the potential and the associated lateral spreading can be significantly slowed (to \sim 20% decrease over a week) by increasing the hydrophobicity of the substrate via the formation of a monolayer of HMDS on the surface of the SiO₂. Calculation of the integrated potentials suggests that lateral spreading is accompanied by some degree of charge dissipation/neutralization (Figure S4 in Supporting information). Also, we observed that the initial rates of decay of negative potentials were typically somewhat (10–20%) faster than the rates for positive potentials. These trends, which are similar those in

corona discharge and contact electrification,^{3,12,29,30} suggest that the underlying processes are mediated by water adsorbed on the surface of the substrate. Counterions, including H₃O⁺, from the condensed water can neutralize some of the printed charge and facilitate its diffusion on the surface.^{3,12} (The e-jet printed charge patterns disappear entirely upon rinsing of the substrate with deionized water.) As further evidence of this mechanism, we observed nearly complete retention of potentials and sizes in patterns of printed dots by storing them in an environment with low humidity (H₂O \sim 0.3 ppm) and exposing to ambient air only for sufficient time (\sim 4 h) for each KFM measurement. As shown in Figure 3g, in such cases the potentials of both positive and negative patterns remained constant for 5 days with negligible lateral spreading. (The \sim 15% decay of the negative potential for the sixth to eighth days resulted primarily for exposure to ambient air during the KFM measurements (Figure S2b in Supporting information).)

The capability of the e-jet printer to select the charge polarity “on the fly” during a single patterning operation enables formation of complex configurations of charge, including in the form of digitized graphic art images, circuit structures, or related, with desired spatial variations in signs and magnitudes of the potentials. As an example, a drawing of Vitruvian man by Leonardo da Vinci was e-jet printed using polyurethane ink with a 1 μ m i.d. nozzle on a HMDS-treated SiO₂ surface. Figure 4a provides an optical image of the result. As shown in the magnified view of the head area (Figure 4b), the image consists of a matrix of dots, with diameters and horizontal spacings of \sim 1.5 and \sim 3 μ m, respectively. The body outline and area inside the circle were printed in PPM and NPM, respectively, as depicted in Figure 4c. An SEM image (with a secondary electron detector) of the pattern appears in Figure 4d. Areas with positive and negative potentials appear darker and brighter, respectively, due to different effects on the electron beam used for imaging (500 eV energy in this case). The number of the secondary electrons that originate from the areas of positive potential is smaller than that from the negative potential regions, as might be expected simply due to electrostatics. This SEM contrast is sufficient to distinguish differences in polarity, at least at a qualitative level, across the entire image, corresponding to areas that are much larger than those that can be examined in a single KFM image. The contrast in the SEM, however, decreases with duration of exposure to the electron beam, likely due to charge neutralization associated with the electrons. Focusing with higher magnification and increasing the beam energy tended to accelerate the rate of this the neutralization. The Vitruvian pattern was scanned using KFM (Figure 4e) before SEM observation, to allow independent identification of the positive and negative regions. The peak potentials, thicknesses, and dot diameters are ca. \pm 5 V, 260 nm, and 2 μ m, respectively. As with the results shown in Figure 3, the potentials are neutralized in locations where the positive and negative charges overlap.

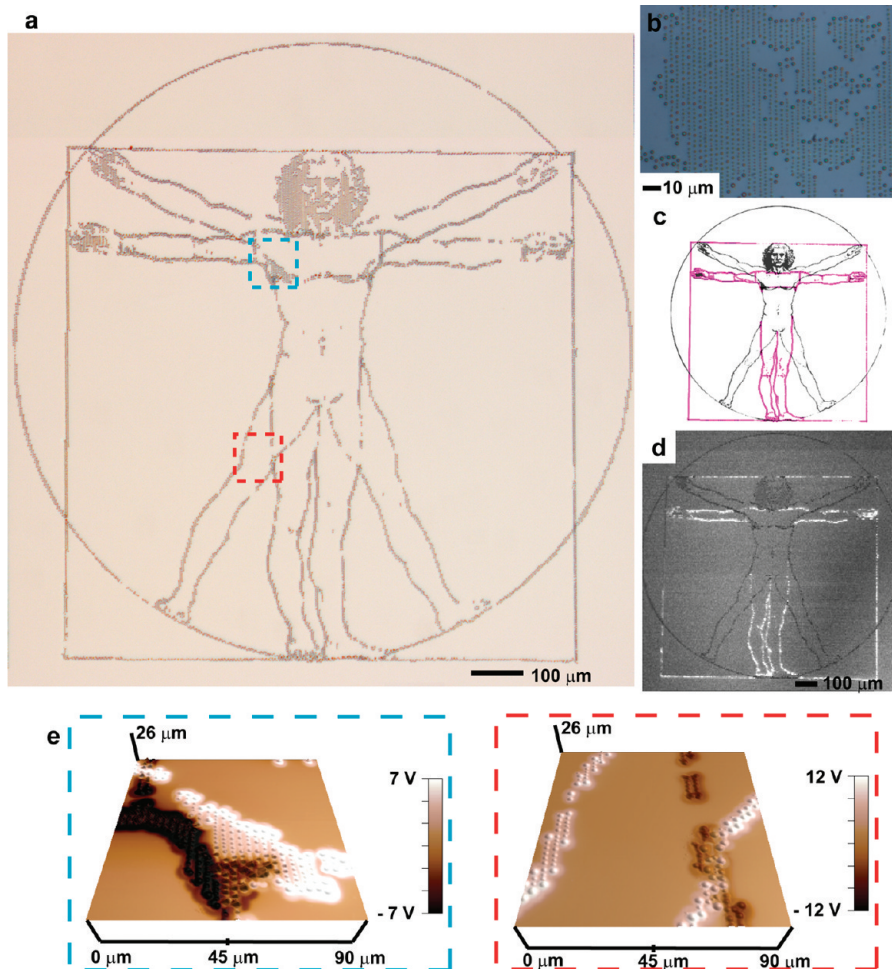


FIGURE 4. Complex image printing with positive and negative charges fully integrated with one another. (a) Optical micrograph of the e-jet printed Vitruvian man. (b) Magnified view of the head area. (c) Original sketch by Leonardo da Vinci (black and red lines indicate areas printed for positive and negative charges, respectively). (d) SEM image of the e-jet printed pattern (positive and negative charges appear dark and bright, respectively). (e) 3D KFM images for blue and red rectangular regions in (a).

To illustrate a different but related capability, Figure S5 in Supporting information shows a printed image of the Apollo statue, in which regions of different charge are separated into stripes. Figure S5a in Supporting information shows an optical micrograph of the printed image and Figure S5b in Supporting information illustrates the areas intended for positive and negative charge. As shown in the KFM image (Figure S5c in Supporting information), these stripes are located immediately next to one another and have potentials of ca. ± 5 V. Similar to the results of Figure 4c, areas with negative potentials appear significantly brighter than the positive regions under the SEM (500 eV).

Such patterns of charge can be used in functional devices. Figure 5 demonstrates an example in the control of properties of silicon nanomembrane transistors. In particular, we use printed charge to pattern regions of electrostatic doping for the purpose of manipulating the threshold voltages, in a manner conceptually similar to recent demonstrations using electrets with organic transistors.^{31–33} In our case, the transistors used 55 nm thick monocrystalline silicon mem-

branes³⁴ formed from the top silicon layer of a silicon-on-insulator wafer, with 145 nm buried SiO₂. Patterned doping with phosphorus provided Ohmic contacts for *n* channel devices with channel lengths and widths of 75 and 100 μm, respectively. The silicon wafer provided a back gate. A 100 nm layer of SiO₂ deposited on top of the silicon in the channel region and treated with HMDS served as a platform for e-jet printed charge. Figure 5a shows a schematic diagram of the device layout and an optical micrograph of representative devices (before printing). Panels b and c of Figure 5 show plots of the drain current (I_d) as a function of the gate voltage (V_g) (at a drain bias, V_d , of 0.1 V) and sets of I_d – V_d curves at various V_g , respectively. The threshold voltage (V_{th}) and the on/off ratio are ca. -6.0 and $\sim 10^6$, respectively. The device mobility evaluated in the linear regime is ~ 600 cm² V⁻¹ s⁻¹. Positive (or negative) charges were printed using e-jet onto the top SiO₂ layer (center part of the device channel, 15 μm away from each edge of S/D), as illustrated in Figure 5d. An aqueous 10 mM sodium chloride ink (10% glycerol added) was used with a 2 μm i.d.

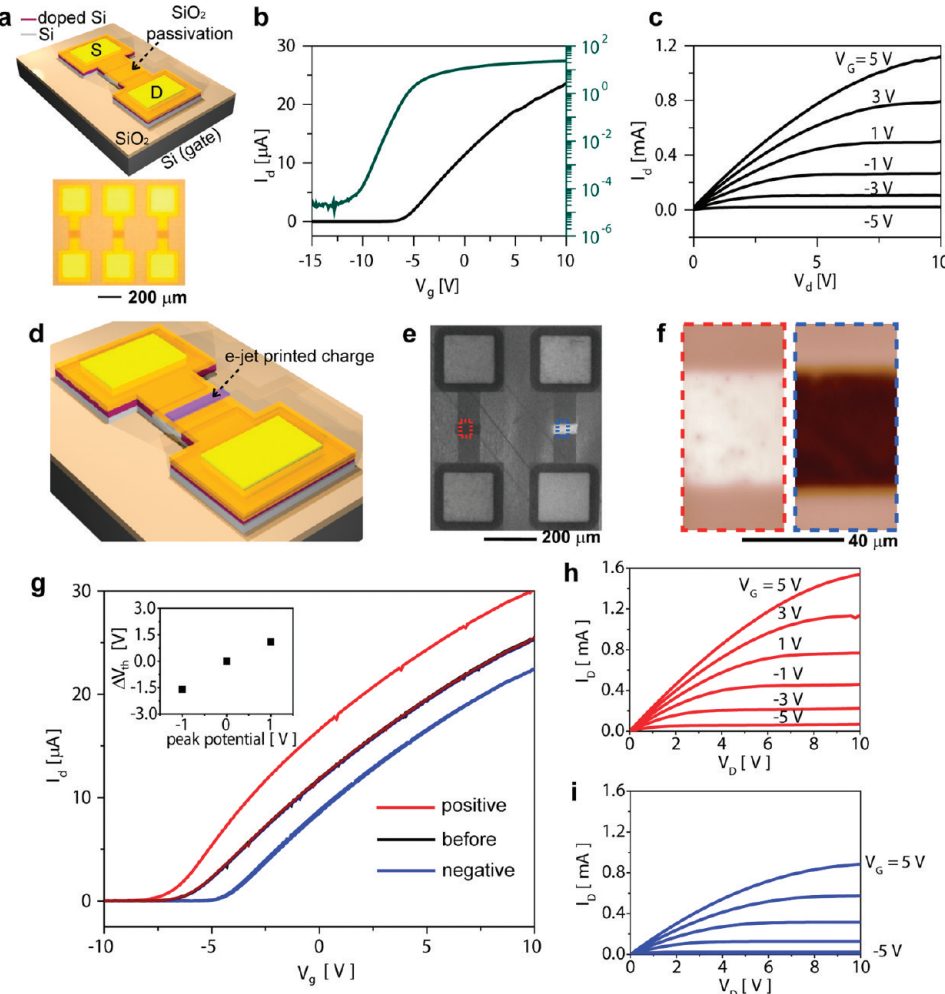


FIGURE 5. Electrostatic doping of silicon nanomembrane transistors using e-jet printed charges. (a) Schematic illustration (top) of the device layout and optical micrograph (bottom) of a set of devices (channel length, 75 μm ; width, 100 μm). (b) V_g - I_d curves at $V_d = 0.1$ V. (c) V_d - I_d characteristics before charge printing. (d) Schematic illustration of charge printed onto the center of the transistor channel coated with a layer of SiO₂. (e) SEM image of channel areas with printed charge (positive and negative charges appear dark and bright, respectively). (f) KFM images of the printed regions (left, +1 V; right, -1 V in peak potentials). (g) Shift of the threshold voltage by the printed charges. (h) positive and (i) negative charges.

nozzle. As shown in the SEM image (Figure 5e), the areas printed with positive charges (or negative charges) appear darker (or brighter) than the nonprinted areas, similar to the cases of Figure 4 and Figure S4 in Supporting information. The peak potentials evaluated by KFM before SEM imaging were +1 or -1 V (Figure 5f). As shown in Figure 5g, V_{th} moves toward the negative (or positive) V_g direction by printing positive (or negative) charges by somewhat more than 1 V in each case (inset of Figure 5g), as might be expected due to the somewhat higher capacitances of the top SiO₂ than the gate dielectric. The I_d - V_d characteristics also change in a consistent manner (Figure 5, parts h and i).

In summary, the work presented here demonstrates that nanoscale electrified fluid jets can be used for high-resolution patterning of charge, to provide capabilities that are unavailable in other methods. Positive and negative potentials with well-defined magnitudes can be printed using various inks, ranging from polymers to metallic nanoparticles, nanowires,

and DNA, and substrate combinations, each with nanoscale resolution. Control over the behavior of silicon nanomembrane transistors provides an example of the use of this method for controlling the properties of nanoscale electronic devices. Developing the technique to allow for even larger potentials and finer features and exploring application opportunities in optoelectronics, sensors, and biotechnology appear to be promising directions for future work.

Acknowledgment. The authors thank H. K. Choi and Professor O. O. Park at KAIST for high-speed imaging of e-jet dynamics and Dr. J. H. Lee and Professor Y. Lu for supplying the DNA suspensions. The authors also acknowledge the Center for Nanoscale Chemical Electrical Mechanical Manufacturing Systems at the University of Illinois, which is funded by National Science Foundation under Grant DMI-0328162. This work was also financially supported by National Research Foundation of Korea (NRF) through a grant (K2070400000307A050000310, Global Research Labo-

ratory (GRL) Program) provided by the Korean Ministry of Education, Science & Technology (MEST) in 2009. Use of the Center for Nanoscale Materials was supported by the U.S. Department of Energy, Office of Science, Office of Basic Energy Sciences, under Contract No. DE-AC02-06CH11357. J.-U.P., S.L., and J.A.R. designed the experiments and wrote the paper. J.-U.P., P.M.F., A.G.A., and J.A.R. contributed to the printer setup, and J.-U.P., and S.L. carried out the ink synthesis, printing, and characterization. S.L., J.-U.P., and S.U. designed device fabrication. Y.G. synthesized suspensions of Ag nanowires and nancubes. J.A.R., U.P., A.G.A., and P.M.F. contributed to project planning.

Supporting Information Available. Details of experiments and additional supplementary figures about the charge dissipations. This material is available free of charge via the Internet at <http://pubs.acs.org>. Correspondence and requests for materials should be addressed to J.A.R. and U.P.

REFERENCES AND NOTES

- (1) Duke, C. B.; Noolandi, J.; Thieret, T. *Surf. Sci.* **2002**, *500*, 1005–1023.
- (2) Pai, D. M.; Springett, B. E. *Rev. Mod. Phys.* **1993**, *65*, 163–211.
- (3) Ressier, L.; Nader V Le., *Nanotechnology* **2008**, *19*, 135301.
- (4) Seemann, L.; Stemmer, A.; Naujoks, N. *Nano Lett.* **2007**, *7*, 3007.
- (5) Mesquida, P.; Stemmer, A. *Adv. Mater.* **2001**, *13*, 1395.
- (6) Tzeng, S.-D.; Lin, K.-J.; Hu, J.-C.; Chen, L.-J.; Gwo, S. *Adv. Mater.* **2006**, *18*, 1147.
- (7) Pingree, L. S. C.; Reid, O. G.; Ginger, D. S. *Adv. Mater.* **2009**, *21*, 19–28.
- (8) Lenggoro, I. W.; Lee, H. M.; Okuyama, K. *J. Colloid Interface Sci.* **2006**, *303*, 124–130.
- (9) Jacobs, H. O.; Whitesides, G. M. *Science* **2001**, *291*, 1763–1766.
- (10) Barry, C. R.; Gu, J.; Jacobs, H. O. *Nano Lett.* **2005**, *5*, 2078.
- (11) Jacobs, H. O.; Campbell, S. A.; Steward, M. G. *Adv. Mater.* **2002**, *14*, 1553.
- (12) McCarty, L. S.; Whitesides, G. M. *Angew. Chem., Int. Ed.* **2008**, *47*, 2188–2207.
- (13) Genda, T.; Tanaka, S.; Esashi, M. *17th IEEE International Conference on Micro Electro Mechanical Systems* **2004**, 470–473.
- (14) Park, J.-U.; et al. *Nat. Mater.* **2007**, *6*, 782–789.
- (15) Park, J.-U.; Lee, J. H.; Paik, U.; Lu, Y.; Rogers, J. A. *Nano Lett.* **2008**, *8*, 4210.
- (16) Choi, H. K.; et al. *Appl. Phys. Lett.* **2008**, *92*, 123109.
- (17) Sekitani, T.; Noguchi, Y.; Zschieschang, U.; Klauk, H.; Someya, T. *Proc. Natl. Acad. Sci. U.S.A.* **2008**, *105*, 4976–4980.
- (18) Taylor, G. I. *Proc. R. Soc. London, Ser. A* **1969**, *313*, 453–475.
- (19) Collins, R. T.; Jones, J. J.; Harris, M. T.; Basaran, O. A. *Nat. Phys.* **2008**, *4*, 149–154.
- (20) Hayati, I.; Bailey, A. I.; Tadros Th., F. *Nature* **1986**, *319*, 41–42.
- (21) Marginean, I.; Nemes, P.; Vertes, A. *Phys. Rev. Lett.* **2006**, *97*, 064502.
- (22) Saville, D. A. *Annu. Rev. Fluid Mech.* **1997**, *29*, 27–64.
- (23) Jurasiche, R.; Rollgen, F. W. *Int. J. Mass. Spectrom.* **1998**, *177*, 1–15.
- (24) Sun, Y.; Xia, Y. *Adv. Mater.* **2002**, *14*, 833–837.
- (25) Lord Rayleigh, *Philos. Mag.* **1882**, *14* (5th), 184–185.
- (26) Marginean, I.; Znamenskiy, V.; Vertes, A. *J. Phys. Chem. B* **2006**, *110*, 6397–6404.
- (27) Gomez, A.; Tang, K. Q. *Phys. Fluids* **1994**, *6*, 404–414.
- (28) Korkut, S.; Saville, D. A.; Aksay, I. A. *Phys. Rev. Lett.* **2008**, *100*, 034503.
- (29) Schönenberger, C. *Phys. Rev. B* **1992**, *45*, 3861–3864.
- (30) Olthuis, W.; Bergveld, P. *IEEE Trans. Electr. Insul.* **1992**, *27*, 691–697.
- (31) Huang, C.; Katz, H. E.; West, J. E. *J. Appl. Phys.* **2006**, *100*, 114512.
- (32) Huang, C.; West, J. E.; Katz, H. E. *Adv. Funct. Mater.* **2007**, *17*, 142.
- (33) Scharnberg, M.; Zaporojtchenko, V.; Adelung, R.; Faupel, F.; Pannemann, C.; Diekmann, T.; Hilleringmann, U. *Appl. Phys. Lett.* **2007**, *90*, 013501.
- (34) Sun, Y.; Choi, W. M.; Jiang, H.; Huang, Y. Y.; Rogers, J. A. *Nat. Nanotechnol.* **2006**, *1*, 201–207.
- (35) Sun, Y.; Xia, Y. *J. Am. Chem. Soc.* **2004**, *126*, 3892.